DOI: 10.13009/EUCASS2022-6122
9TH EUROPEAN CONFERENCE FOR AERONAUTICS AND SPACE SCIENCES (EUCASS)

Low-order models for acoustic modes in a ramjet combustor with inlet shock train

Erwin Bekaert[⋆†], *Aurelien Genot*[⋆], *Thomas Le Pichon*[⋆], *Thierry Schuller*[*]
[⋆]*DMPE, ONERA, Université Paris Saclay, F-91123 Palaiseau - France*
[*]*Institut de Mécanique des Fluides de Toulouse, IMFT, Université de Toulouse, CNRS, Toulouse, France*
erwin.bekaert@onera.fr
[†]Corresponding author

Abstract

The acoustic field inside a model ramjet combustor featuring a low frequency combustion instability is investigated with a set of low-order models of increasing complexity. Under the conditions investigated, the ramjet features a shocked flow at the combustion chamber nozzle outlet and a shock train at its air inlets characterized by a displacement synchronized with the combustion oscillation. The objective is to understand by which acoustic boundary condition the moving shock train can be replaced to model the downstream acoustic field. Four analytical models are tested and compared to POD results from LES data. Models 1 and 2 consider a fixed shock that respectively behaves as a pressure node and a velocity node. Model 3 includes the displacement of the shock due to pressure disturbances inside the combustion chamber. Finally, model 4 also takes into account effects of the mean flow velocity on the acoustic field. From these comparisons, it is concluded that a moving velocity node reproduces a better shape of the mode in the vicinity of the shock train than a pressure release. Moreover, model 4 that includes mean flow effects yields a similar frequency and a similar mode shape in the vicinity of the shock train as in the data from numerical simulations. However, a closer comparison with these data shows that the model fails to reproduce the deformation and the magnitude of displacement of the mode and suggests that a more complex dynamics needs to be considered.

Introduction

As many other propulsion systems including gas turbines, solid rocket motors, and liquid-propellant rockets, ramjets extreme operating conditions facilitate the triggering of combustion instabilities which can lead to premature extinctions, chamber damages and in the worst cases a destruction of the engine. In many cases, ramjets develop thermo-acoustic instabilities [13, 12, 7, 9] resulting from a resonant coupling between the combustion dynamics and one of the eigenmode of the engine cavities [4] that lead to large synchronized periodic oscillations of flow inside the ramjet.

The variety of physical phenomena involved makes the prediction of thermo-acoustic instabilities challenging at the design stage of a combustor which is frequently based on empirical testing methods to avoid these spurious oscillations. Large eddy simulations (LES) have been performed on several configurations and tend to show a growing capability at reproducing thermo-acoustic instabilities in real combustors [8]. However, these simulations of the unsteady reacting flow inside a ramjet are extremely expensive and rely on the use of massively parallel computation resources that cannot be envisaged for parametric analysis at industrial development scales. An alternative is to use low-order models to represent the interaction between the acoustic field and the combustion dynamics at a reduced computational cost in order to approach reference values given by experiments or by detailed numerical flow simulations.

Thermo-acoustic instabilities have been identified in the ONERA experimental bench '*Research Ramjet*', in French *Statoéacteur de Recherche (SdR)*. The SdR is a two-inlet side-dump combustor, which can be operated with gaseous or liquid fuels for operating conditions that are representative of flight conditions [10, 7]. The rectangular air inlets shown on the setup in Fig. 1 are simplified compared to a flight vehicle; however, as in real diffusers, a train of shock waves develops downstream the air inlet sonic throats.

By applying Proper Orthogonal Decomposition (POD) to results from LES simulations of the SdR [11, 15], two dominant longitudinal modes could be identified during thermo-acoustic instability, mode 1 at 110 Hz and mode 3

DOI: 10.13009/EUCASS2022-6122

at 393 Hz. Mode 3 was found to originate from pressure waves radiated from the combustion region that propagate upstream toward the air inlet shocks and downstream toward the combustion chamber shocked nozzle. It is known that a shock does not remain stable when submitted to downstream fluctuations and that its structure and its position change [2, 1, 3]. This is corroborated by the POD analysis that confirms that the shock train at the air inlet substantially alters the acoustic field inside the ramjet. An attempt is made in this study to develop a low order model of the shock train and reproduce the acoustic field inside the ramjet. The problems more specifically considered herein are: How to describe the air inlet shock train as a boundary condition in an acoustic model of the ramjet cavity? How this acoustic description of the shock influences the acoustic modal shape inside the ramjet?

Four low-order models of increasing complexity are tested to reproduce the acoustic field inside the ramjet observed for mode 3. The simplified low-order model framework used in this study is described in section 1. Two models are then introduced in section 2 for a shock treated as a fixed boundary condition. The last two models in section 3 consider a moving shock and include effects of the mean flow. Results for the different models are compared in section 4.

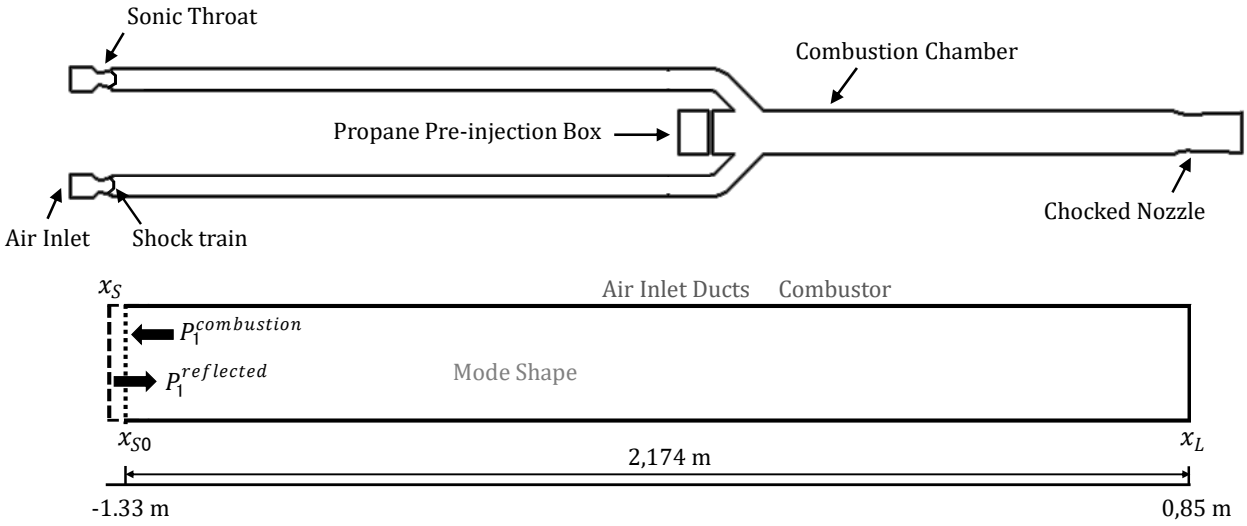

Figure 1: *Top*: Sketch of the ONERA *Research Ramjet* (SdR) in gaseous fuel operating conditions. *Bottom*: Schematic of the low-order models developed in this study.

1. Simplified model of the ramjet acoustics

To study the dynamics of the longitudinal mode 3 that is triggered inside the ramjet during self-sustained combustion oscillations, a set of simplifications is made:
(1) The shock train that develops downstream the sonic nozzle throat inside the air inlets is replaced by a normal shock stabilized in a section inside the diverging channel [3].
(2) This normal shock constitutes one boundary condition of the acoustic model set at $x = x_{S0}$.
(3) The sonic flow at the nozzle throat at the combustion chamber outlet is replaced by an acoustic velocity node at $x = x_L$ [6].
(4) As the structure of mode 3 corresponds to a pressure oscillation controlled by the reflection of sound waves at the shock train and at the combustion chamber nozzle exhaust, the SdR geometry is simplified and treated as a one dimensional duct as shown in Fig. 1 with only longitudinal waves propagating along the x axis.
(5) The impact of steady combustion and of temperature gradients are neglected and the sound speed is assumed to be constant through the cross section area of the acoustic model which is also assumed to be constant.
(6) Acoustic losses and acoustic sources, in particular the impact of unsteady combustion [14, 5], are neglected.
This simplified model cannot reproduce the complexity of the dynamics observed inside the ramjet and is only used here to understand how to mimic the impact of the shock train on the mode shape observed in the simulations.

The governing equations assume small acoustic perturbations in an isothermal inviscid non-reacting flow with a constant flow velocity u_0. In these conditions, the advected wave equation for acoustic pressure disturbances p_1 takes

DOI: 10.13009/EUCASS2022-6122

the form:

$$(c_0^2 - u_0^2)\frac{\partial^2 p_1}{\partial x^2} - \frac{\partial^2 p_1}{\partial t^2} - 2u_0\frac{\partial^2 p_1}{\partial x \partial t} = 0 \tag{1}$$

In the cases where the Mach number remains small, the mean flow velocity u_0 can be neglected and one is left with the standard wave equation:

$$c_0^2\frac{\partial^2 p_1}{\partial x^2} - \frac{\partial^2 p_1}{\partial t^2} = 0 \tag{2}$$

This last approximation is retained in section 2 while Eq. (1) is used in section 3. Solutions of Eqs. (1) or (2) are sought with the Galerkin decomposition [4, 5, 16]:

$$p_1(x,t) = \mathrm{Re}\left\{\sum_n \eta_n(t)\Psi_n(x)\right\} \tag{3}$$

where the complex eigenmodes $\Psi_n(x)$, with n being the number of the mode, form an orthogonal basis and comply with the boundary conditions of the problem. The complex mode amplitude $\eta_n(t)$ is given by [4]:

$$\frac{\partial^2 \eta_n}{\partial t^2} + \omega_n^2 \eta_n = 0 \tag{4}$$

where $\omega_n = 2\pi f_n$ is the angular frequency. In the case of a low Mach flow, the modes Ψ_n are solutions of the Helmholtz equation [4]:

$$\frac{\partial^2 \Psi_n}{\partial x^2} + k_n^2 \Psi_n = 0 \tag{5}$$

with the wave number $k_n = \omega_n / c_0$. Solutions of Eqs. (4) and (5) are the harmonic functions:

$$\Psi_n(x) = P_{+n}\exp(ik_n x) + P_{-n}\exp(-ik_n x) \tag{6}$$

$$\eta_n(t) = A_n\exp(-i\omega_n t) + B_n\exp(i\omega_n t) \tag{7}$$

The complex coefficients A_n and B_n only depend on the initial condition and P_+ and P_- depend on the acoustic boundary conditions at $x = x_{s0}$ and $x = x_L$. By further assuming that $p_1 = 0$ at $t = 0$, one is left with $\eta_n(t) = 2C_n i \sin(\omega_n t)$, where C_n is an arbitrary complex coefficient.

This simplified framework is used in the following to test different boundary conditions for the shock train at $x = x_{S0}$ and examine the acoustic pressure field inside the model ramjet.

2. Standing waves for a fixed shock train

Effects of the mean flow u_0 are neglected in this section. The response of the ramjet outlet at the sonic nozzle throat at $x = x_L$ is approximated by a velocity node where $u_1(x_L) = 0$. In this section, the location of the shock inside the air inlet at $x = x_{S0}$ is assumed to be fixed and insensitive to pressure disturbances inside the ramjet. In this case, the geometry of the cavity remains fixed and a standing wave develops in the cavity: the wave oscillates in time but its amplitude peaks have fixed positions in space. Two different limit cases are tested.

2.1 Model 1 SW O-R: Standing Wave, Open-Rigid boundaries

In the first model, a pressure release $p_1 = 0$ is imposed at $x = x_S = x_{S0}$ as if the shock acted as a large pressure tank with a vanishingly small impedance when perturbed from the downstream side leading to the following boundary conditions:

$$p_1(x = x_S) = 0 \quad \text{and} \quad u_1(x_L) = 0 \tag{8}$$

The solution of the problem is:

$$p_{1n}(x,t) = \mathrm{Re}\{\eta_n \Psi_n\} = D_n \sin(\omega_n t)\left(\sin(k_n x - 2k_n x_S) + \sin(k_n x)\right) \tag{9}$$

where $k_n = (2n+1)\pi/(2(x_L - x_S))$ with $n = 0, 1, 2...$ and D_n is the mode amplitude.

DOI: 10.13009/EUCASS2022-6122

2.2 Model 2 SW R-R: Standing Wave, Rigid-Rigid boundaries

The second model considers that a normal shock acts like a rigid wall for pressure perturbations downstream the shock by imposing $u_1 = 0$ at $x = x_S$. This model assumes that the normal shock cannot adapt instantaneously to pressure fluctuations and features an infinite impedance in which case the boundary conditions are now:

$$u_1(x_S) = 0 \quad \text{and} \quad u_1(x_L) = 0 \tag{10}$$

The solution now writes:

$$p_{1n}(x,t) = \mathrm{Re}\{\eta_n \Psi_n\} = E_n \sin(\omega_n t)\,(\sin(2k_n x_S - k_n x) + \sin(k_n x)) \tag{11}$$

and the wave number is given by $k_n = n\pi/((x_L - x_S))$.

3. Traveling waves for a moving shock train

In reality, the shock train position inside the air intakes depends on the downstream pressure. As this pressure fluctuates in time due to the self-sustained combustion oscillation, the position of the equivalent normal shock at $x = x_S$ is now also assumed to fluctuate around the position without any fluctuation $x = x_{S0}$. Since one of the acoustic boundary of the problem is now moving, solutions of the wave equation do not correspond anymore to standing waves, but traveling waves must be considered.

3.1 Model 3 TW R-R: Traveling-Wave, Rigid-Rigid boundaries

In model 3, the mean flow u_0 is still neglected and the shock is assumed to behave as a rigid wall as in model 2. However, it is assumed that the shock position $x_S(t)$ now also responds linearly to downstream harmonic pressure fluctuations p_1 inside the ramjet combustion chamber by an harmonic displacement of the normal shock position $x_s(t)$ around its position x_{S0} without fluctuation. Culick and Rogers [3] expression for the displacement of a normal shock under the action of an imposed oscillating external pressure p_1 in a channel of constant cross-section is retained to model this behavior:

$$\frac{\mathrm{d}x_S(t)}{\mathrm{d}t} = -\frac{c_{0u}}{\rho_{0u}} \frac{(\gamma+1)}{4\gamma M_{0u}} p_1(x,t) \tag{12}$$

The subscript u corresponds to values of the flow variables taken just upstream the shock wave, where ρ_0 is the unperturbed flow density and γ the specific heat capacity ratio of the gases.

To further simplify the problem, a quasi-steady approximation is made for the motion of the acoustic boundary at $x = x_S(t)$ with respect to the oscillation period $T_n = 2\pi/\omega_n$ of the acoustic pressure field inside the ramjet. With this questionable but convenient hypothesis, the pressure field can be deduced from Eq. (11) for a duct closed by rigid walls at its two boundaries:

$$p_{1n}(x,t) = \mathrm{Re}\{\eta_n \Psi_n\} = E_n \sin(\omega_n t)\Big(\sin(2k_n x_S(t) - k_n x) + \sin(k_n x)\Big) \tag{13}$$

This expression for the pressure field p_1 combined with Eq. (12) indicates that the shock displacement Δx_S around the position x_{S0} is given by:

$$x_S(t) = x_{S0} - \Delta x_S \cos(\omega_n t) \tag{14}$$

where the amplitude Δx_S of the shock displacement is limited by the location of the nozzle throat. This displacement is also estimated from LES results [11].

3.2 Model 4 TW R-R M: Traveling Wave, Rigid-Rigid boundaries, Mean flow

In the configuration explored, the average Mach number M_0 of the mean flow inside the ramjet between x_S and x_L is $M_0 = 0.3$, for a mean sound speed $c_0 = 600\ m.s^{-1}$. Hence it is relevant to take into account effects of the mean flow on the previous results.

In this case, the mode shape becomes:

$$\Psi_n(x) = P_{+n} \exp\left(i \frac{k_n}{1+M_0} x\right) + P_{-n} \exp\left(i \frac{k_n}{1-M_0} x\right) \tag{15}$$

DOI: 10.13009/EUCASS2022-6122

With the acoustic boundary conditions at $u_1(x_S(t)) = 0$ and $u_1(x_L) = 0$ and the same hypothesis as for model 3, it comes for the pressure fluctuations p_1 inside the ramjet:

$$p_{1n}(x,t) = F_n \sin(\omega_n t)\left(\sin\left(\frac{k_n}{1+M_0}x_S(t) + \frac{k_n}{1-M_0}x_S(t) - \frac{k_n}{1+M_0}x\right) + \sin\left(\frac{k_n}{1-M_0}x\right)\right) \tag{16}$$

with F_n the amplitude of the pressure perturbation and:

$$k_n = \frac{n\pi(1-M_0^2)}{(x_L - x_S(t))} \tag{17}$$

Including advection due to the mean flow velocity does not modify the expression of $x_s(t)$ from Eq. (14).

4. Model comparisons

For the considered operating condition of the SdR, a self-sustained oscillation predominantly associated to mode 3 with a corresponding frequency of 393 Hz was identified in the LES [11]. The structure of the pressure fluctuations p_1 associated to this mode is plotted in Fig. (2) along the ramjet. This figure has been extracted from Anthony Roux PhD thesis with legends in French. Two zones are indicated in this figure. The first one, 'Entrées d'air' corresponds to the air inlet ducts. The second one 'Chambre de combustion' delineates the span of the combustion chamber. From the position of the shock train near $x = -1.33$ m one can identify a first pressure node roughly around $x = -1.13$ m. A closer look indicates that the pressure signals plotted at different instants in the oscillation cycle do not cross at a fixed point. The pressure wave field indeed slightly translates with the same shift in position as the motion of the inlet shock train. There is a second nodal line close to the middle of the combustion chamber roughly around $x = 0.06$ m. The displacement of this pressure node has a higher amplitude than the motion of the first pressure node. Finally, the influence of the chocked nozzle at the chamber outlet on the mode shape is noticeable at the exit of the combustor.

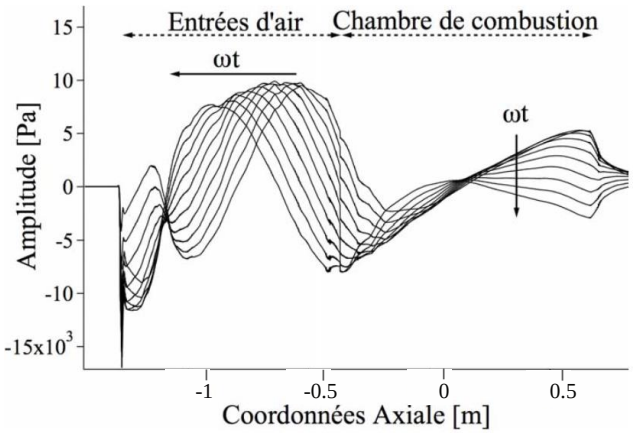

Figure 2: Temporal evolution of the spatial structure of pressure fluctuations p_1 corresponding to mode 3. LES from [11]

Table 1 compares the first five modes identified in the LES [11] characterized by their frequency. These frequencies are compared to the predictions from the four analytical models presented in sections 2 and 3.
Frequencies in bold in Table 1 are the ones that match better the values provided by LES. The best results are obtained with model 4 (TW R-R M)), corresponding to a cavity closed at both boundaries when mean flow effects are taken into consideration. This table also clearly shows that model 2 (SW R-R) featuring a fixed cavity size and model 3 (TW R-R) featuring the same boundary conditions as model 2 but with a fluctuating size due to a small motion of the inlet boundary yield the same frequency distributions. Indeed the motion altering the cavity size remains small compared to the length $L = 2.17$ m of the cavity.

The pressure distribution for mode 3 is plotted in Fig. 3 for model 1 and model 2. In these plots and the following ones, the blue vertical dashed line at $x = -1.366$ m stands for the throat of the sonic nozzle inside the air inlet ducts.

DOI: 10.13009/EUCASS2022-6122

Table 1: *Left:* Frequencies of acoustic modes (Hz) identified in the LES [11]. *Right:* Frequencies predicted by model 1 (SW O-R), model 2 (SW R-R), model 3 (TW R-R) and and model 4 (TW R-R M).

Mode	LES [11]	SW O-R	SW R-R	TW R-R	TW R-R M
1	110	69	138	138	**126**
2	222	**207**	276	276	**251**
3	393	345	**414**	**414**	**377**
4	510	483	552	552	**502**
5	960	621	690	690	628

Likewise, the black vertical dotted lines at $x = -1.332$ m and $x = 0.842$ m correspond to the locations of the acoustic boundary conditions, i.e. the position of the normal shock wave and the position of the sonic nozzle throat at the ramjet combustion chamber exhaust. Comparing the shape of mode 3 obtained by these two models with the results shown in Fig. 2, model 1 considering an open boundary condition at $x = x_S$ does not reproduce the correct behavior near the shock. Results from numerical simulations indicate large pressure disturbances at $x = x_S$ meaning that the shock train response is closer to model 2 corresponding to a rigid acoustic boundary at $x = x_S$ where p_1 is maximum. There are however two main differences between Fig. 3 with LES results plotted in Fig. 2. The first one is that the two peaks on the right plot in Fig. 3 have the same amplitude whereas LES, predicts a higher amplitude for the first peak. The second difference is pressure fluctuation at the ramjet exhaust nozzle. In model 2, it also corresponds to a maximum of pressure oscillation because it is modeled as velocity node, but in the LES, the pressure fluctuation level is reduced compared to the maximum fluctuation level observed inside the air inlets.

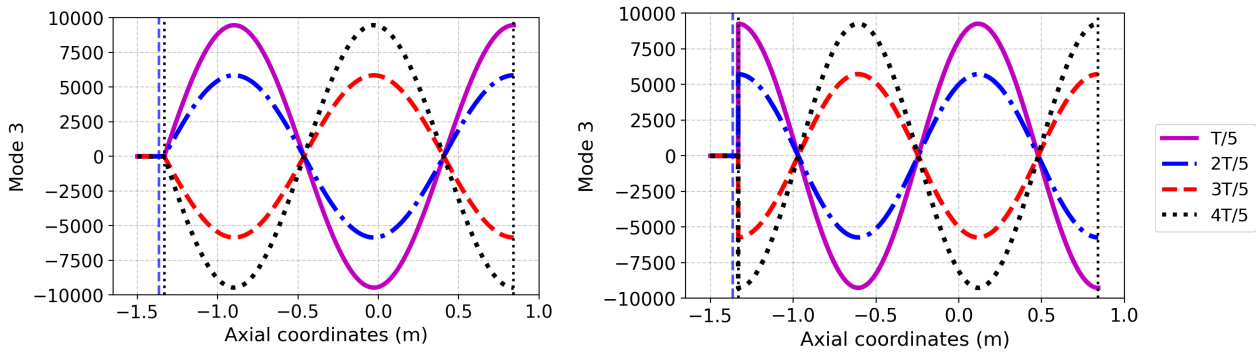

Figure 3: Evolution of pressure fluctuations p_1 for mode 3 over a period of oscillation at $t/T = 1/5$, $t/T = 2/5$, $t/T = 3/5$ and $t/T = 4/5$ with, *left:* model 1 SW O-R with open-rigid acoustic boundaries, *right:* model 2 SW R-R with rigid-rigid acoustic boundaries.

Results are now plotted for model 3 in Fig. 4 when the moving rigid wall boundary is taken into account. In these plots the normal shock moves harmonically according to Eq. (14). As suspected, the shape of the mode is almost identical to that found on the right plot in Fig. 3. Indeed, it is delicate to see any difference between the two modal distribution on the right in Fig. 3 and in Fig. 4 because the amplitude of motion of the rigid boundary remains small 0.040 m compared to the length 2.174 m of the domain. Hence, the small motion of the mode is hardly perceptible. A zoom in the neighborhood of the shock is presented on the right in Fig. 4. This zoom allows to apprehend the shock motion around x_{S0}. It is recalled that the blue vertical dashed line corresponds to the throat of the nozzle and the black vertical dotted line represents the position of the steady shock, without pressure fluctuations, x_{S0}. On the upstream side of the shock position, $p_1 = 0$, there are no pressure fluctuations beyond the $M = 1$ isoline in the supersonic region of the flow. Moreover, the shock never reaches the throat of the nozzle since its maximum displacement is at $x = -1.352$ m. Figure 4 also shows that the pressure nodes are not fixed in space. As all the mode slightly moves with the boundary condition, pressure nodes are not defined at a fixed location. The magnitude of the displacement of the fist pressure node obtained by the moving the boundary condition is similar to the one observed in the LES and is of the order of 2 cm. Nevertheless, the predicted amplitude of displacement of the second pressure node inside the combustion chamber is smaller than the displacement of the first node with model 3 whereas the opposite is observed in the LES. Moreover, another difference with LES results is that the displacement predicted by the model remains too

DOI: 10.13009/EUCASS2022-6122

small. These differences may originate from the impact of the combustion reaction that is not taken into account in the model.

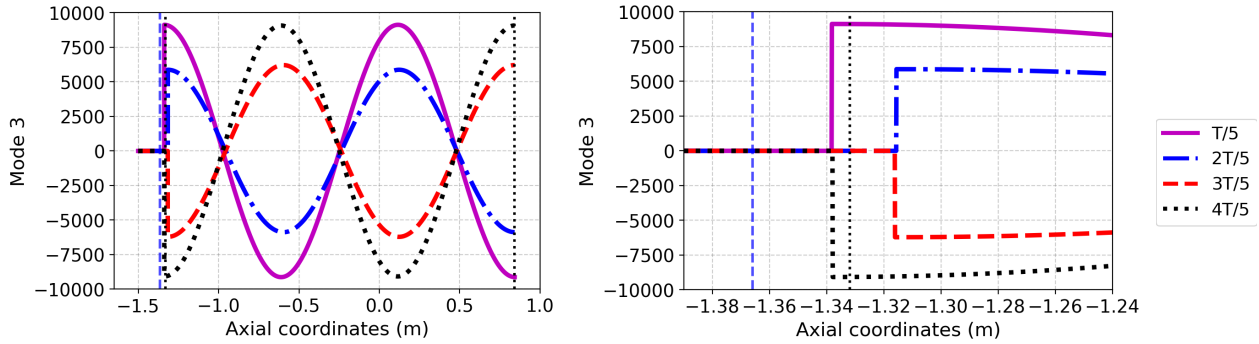

Figure 4: Evolution of pressure fluctuations p_1 for mode 3 over a period of oscillation of the normal shock position at $t = \frac{T}{5}$, $t = \frac{2T}{5}$, $t = \frac{3T}{5}$ and $t = \frac{4T}{5}$ with the moving rigid-rigid wall model. *Left:* complete geometry. *Right:* focus on the vicinity of the normal shock.

Predictions with model 4 corresponding to a rigid cavity at both boundaries but including the motion of the normal shock at the inlet and effects of the mean flow are presented in Fig. 5. The shape of the mode now differs from predictions with model 3 shown in Fig. 4. In this model, the highest pressure disturbances are only observed at the boundaries. The other two peaks in the center of the ramjet do not reach the same fluctuation levels. This is also corroborated in the LES [11]. In the first half of the domain, the results with model 4 are very similar to those found with LES: the maximum pressure fluctuation is reached at the shock location followed by a weaker peak in phase opposition at the first quarter of the domain. However, in the second half of the domain, model 4 predictions and LES results substantially deviate. Results obtained for the motion of the shock being identical to the ones found with model 3 they are therefore not represented. As for model 3, the whole mode slightly moves with the motion of the boundary condition and the pressure nodes are not fixed in space as also observed in the LES. However, the displacement of the pressure nodes is clearly not of the same order of magnitude of the displacements observed in LES. The acoustic mode deformation observed in LES is not well reproduced by any of the four models tested.

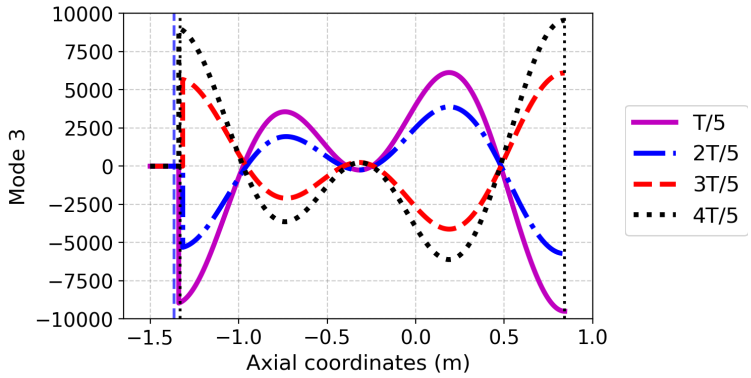

Figure 5: Evolution of pressure fluctuations p_1 for mode 3 over a period of oscillation of the normal shock position at $t = \frac{T}{5}$, $t = \frac{2T}{5}$, $t = \frac{3T}{5}$ and $t = \frac{4T}{5}$ with the moving rigid-rigid wall model with mean flow effects.

This analysis shows that a moving acoustic boundary condition modeling the shock train motion is not sufficient enough to reproduce the mode shape deformation observed in LES suggesting that a more complex dynamics has to be taken into consideration.

DOI: 10.13009/EUCASS2022-6122

5. Conclusion

In this study, four simplified models have been developed to represent the acoustic pressure distribution in a ramjet with air inlet shock trains. Previsions of the models have been compared to LES results [11] and four principal elements were highlighted:

(1) A satisfying qualitative representation of the acoustic field in the ramjet can be obtained by modeling the air inlet shock trains as a velocity node.
(2) Taking into consideration the shock train movement due to downstream pressure fluctuations does not significantly change the modal distribution in the combustor since the amplitude of motion of the shock trains remains small compared to the length of the global system.
(3) Mean flow effects inside the combustor has to be taken into consideration since it was proved to have an influence on the pressure mode shapes and on the corresponding frequency values.
(4) The exit chocked nozzle represented in the models as a velocity node is not sufficient enough to reproduce the modal distribution in the combustion chamber.

Thanks to previous results from our basic models, some potential key elements can be identified in order to improve and extend validity of the existing models. Taking into consideration different zones where the speed of sound could vary could locally deform the mode shape and help to match the mode shape provided by LES. Moreover, a change of the cross-section throughout the geometry could be taken into consideration. Finally, as previously mentioned, the rigid wall boundary condition to model the behavior of the chocked exit nozzle in not sufficient enough, a better representation of its behavior could have a non-neglecting impact on the modal distribution inside the combustor.

Acknowledgments

The authors gracefully aknowledge A. K. Mohamed, O. Dessornes, J. Anthoine, P. Villedieu, L. Jacquin from ONERA and M. Voisine from DGA for their support, as well as ONERA and AID for their financial support.

References

[1] P.J.K. Bruce and H. Babinsky. Unsteady shock wave dynamics. *Journal of Fluid Mechanics*, 603:463–473, 2008.

[2] R. Bur, R. Benay, A. Galli, and P. Berthouze. Experimental and numerical study of forced shock-wave oscillations in a transonic channel. 2003.

[3] F.E.C. Culick and T. Rogers. The response of normal shocks in diffusers. *AIAA Journal*, 21:1382–1390, 1981.

[4] F.E.C. Culick and V. Yang. Prediction of the stability of unsteady motions in solid-propellant rocket motors. 1990.

[5] T. Lieuwen. *Unsteady combustor physics*.

[6] F.E. Marble and S. Candel. Acoustic disturbance from gas non-uniformities convected through a nozzle. *Journal of Sound and Vibration*, 55:225–243, 1977.

[7] T. Le Pichon and A. Laverdant. Numerical simulation of reactive flows in ramjet type combustors and associated validation experiments. *AerospaceLab Journal*, 11, 2016.

[8] T. Poinsot. Prediction and control of combustion instabilities in real engines. *Proceedings of the Combustion Institute*, 36:1–28, 2017.

[9] S. Reichstadt. *Etude du mélange et de la combustion monophasique dans un statoréacteur de recherche*. PhD thesis, Université de Pau et des pays de l'Adour, 2007.

[10] A. Ristori and A. Cochet. Research ramjet program: an initiative to improve knowledge on ramjet reactive flowfields. *4^{th}Onera/DLR Aerospace Symposium*, 2002.

DOI: 10.13009/EUCASS2022-6122

[11] A. Roux. *Simulation aux Grandes Echelles d'un statoréacteur*. PhD thesis, Université de Toulouse, 2009.

[12] A. Roux, L.Y.M. Gicquel, S. Reichstadt, N. Bertier, G. Staffelbach, F. Vuillot, and T.J. Poinsot. Analysis of unsteady reacting flows and impact of chemistry description in large eddy simulations of side-dump ramjet combustors. *Combustion and Flame*, 157:176–191, 2010.

[13] A. Roux, S. Reichstadt, N. Bertier, L. Gicquel, F. Vuillot, and T. Poinsot. Comparison of numerical methods and combustion models for les of a ramjet. *Compte Rendus Mécanique*, 337:352–361, 2009.

[14] T. Schuller, T. Poinsot, and S. Candel. Dynamics and control of premixed combustion systems based on flame transfer and describing functions. *Journal of Fluid Mechanics*, 894, 2020.

[15] A. Towne, O.T. Schmidt, and T. Colonius. Spectral proper orthogonal decomposition and its relationship to dynamic mode decomposition and resolvent analysis. *Journal of Fluid Mechanics*, 847:821–867, 2018.

[16] V. Yang, S. Kim, and F.E.C. Culick. Triggering of longitudinal pressure oscillations in combustion chambers. i, nonlinear gas dynamics. *Combustion Science and Technology*, 72:183–214, 1990.